

**THE INTERIOR OF SHACKLETON CRATER AS REVEALED BY MINI-RF ORBITAL RADAR.** B. J. Thomson<sup>1</sup>, D. B. J. Bussey<sup>1</sup>, J. T. S. Cahill<sup>1</sup>, C. Neish<sup>1</sup>, G. W. Patterson<sup>1</sup>, and P. D. Spudis<sup>2</sup>, <sup>1</sup>JHU Applied Physics Lab, Laurel MD 20723, <sup>2</sup>Lunar and Planetary Institute, Houston TX 77058, (bradley.thomson@jhuapl.edu).

**Introduction:** Given the low inclination of the Moon's rotational axis to the normal of the ecliptic plane ( $1.6^\circ$ ), impact craters near the north and south poles receive extremes of solar insolation and therefore contain unique geologic environments. Certain topographically elevated points in the rim crest of polar craters receive near-continuous sunlight over the course of a 28-day lunar diurnal cycle [1]. Conversely, many interior regions of polar craters lie in permanent shadow and thus may represent sites of lunar volatile accumulation [e.g., 2, 3, 4].

With an active source, imaging radars can effectively "see in the dark." However, from an Earth-based viewing geometry, much of the interiors of these craters are hidden from view. The radar instrument Mini-RF onboard NASA's Lunar Reconnaissance Orbiter (LRO) provides an opportunity to view these craters from a more favorable orbital geometry. Here we report on Mini-RF observations of Shackleton crater near the lunar south pole.

**Background:** With a diameter of 20 km, Shackleton is the largest impact crater located within  $1^\circ$  of the south pole of the Moon. The lunar geographic pole lies on the rim crest of Shackleton Crater, which itself is situated on an inner rim massif of the much larger South Pole-Aitken Basin (2600 km in diameter) [5]. Coarse-resolution bistatic radar measurements from the Clementine mission show a polarization signature consistent with water ice over the lunar south polar region (including Shackleton) [6], although this interpretation has been disputed [7]. Higher resolution images from ground-based radar reveal that some areas with high circular polarization ratios (CPR) lie inside the rim of Shackleton, and regions with thick ice deposits are expected to have  $CPR > 1$ . However, these near-rim regions receive at least seasonal illumination, and thus are geologically inconsistent with volatile accumulation in a cold trap [8].

Mini-RF is a dual-band, synthetic aperture radar (SAR) onboard LRO [9, 10] operating in the S-band (2.38 GHz, 12.6 cm wavelength) and X-band (7.14 GHz, 4.2 cm wavelength). Here we concentrate on the S-Band data acquired in zoom mode (pixel spacing of 15 m). Due to the proximity of Shackleton Crater to the pole, the LRO spacecraft conducted small rolls toward nadir ( $14\text{--}19^\circ$ ) from the nominal incidence angle of  $\sim 48^\circ$  to bring the crater into the radar field of view. Rolled observations of Shackleton were con-

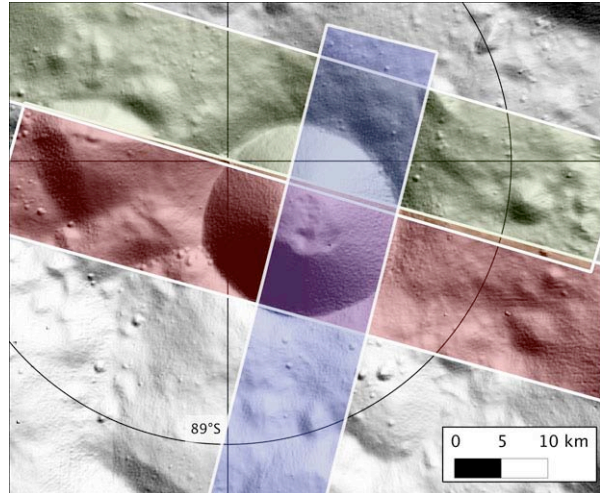


**Figure 1.** Topographic shaded relief map from LOLA gridded data [11] of the south polar region. The position of Mini-RF data swaths over Shackleton crater are indicated by colored boxes.

ducted on 23 Dec. 2009, 18 Apr. 2010, and 26 Jun. 2010 (Fig. 1).

**Method:** Inherent in the oblique viewing geometry of a SAR instrument is a parallax distortion introduced by terrain height variations. This topography-induced distortion causes points above the surrounding surface to be displaced in the near-range direction of the sensor; low topographic points are displaced toward the far range. Using a 256 ppd gridded topographic dataset from the Lunar Orbiter Laser Altimeter (LOLA) instrument [11], we have corrected for this effect on a pixel-by-pixel basis. The resulting corrected radar swaths were analyzed to determine the variation in observed radar properties with local inci-

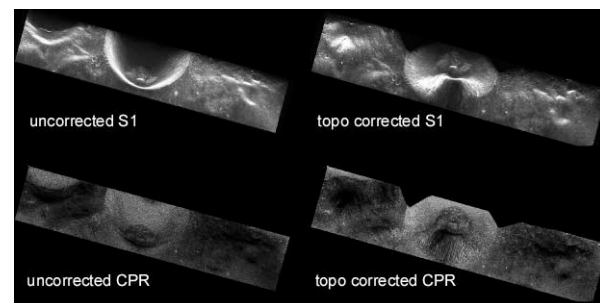


**Figure 2.** Comparison of uncorrected (left) and topographically corrected version (right) of Mini-RF swath LSZ\_03737\_2CD\_OKU\_90S137\_V1 acquired over Shackleton Crater.

dence angle.

**Results:** Corrected and uncorrected perspectives of a Mini-RF radar swath over Shackleton are given in Fig. 2 for the radar Stokes parameter ( $S_1$ ) and the circular polarization ratio (CPR).  $S_1$  is the total radar backscatter from the lunar surface, while CPR is the ratio of same sense to opposite sense circular polarization. In the uncorrected version, the floor of the crater is displaced away from the observer (toward the bottom of the scene). In the processed version, the floor of the crater is restored to its true center location.

To further characterize the crater's interior radar signal, we extracted CPR values and other radar parameters from three concentric rings: an upper, middle, and lower ring (Fig. 3a). The upper ring is located on the inner wall slope just inside the crater rim crest, and the lower ring is located just above the flat to hummocky crater floor. The middle ring is located between these two.

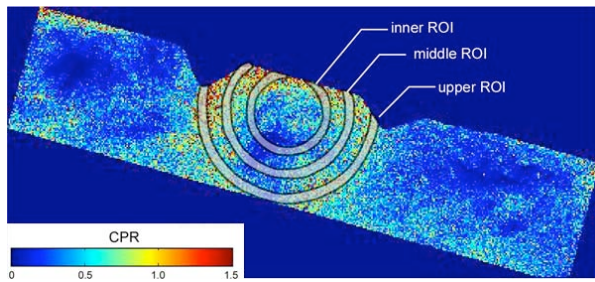
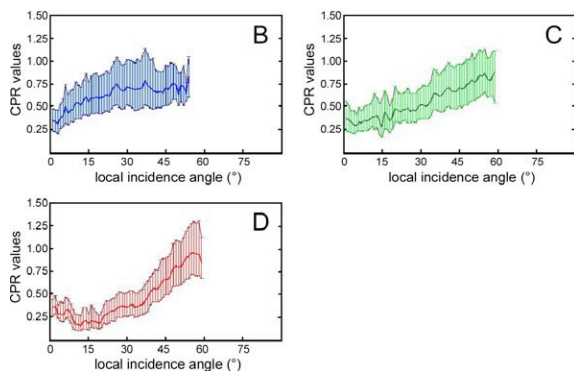


**Figure 3a.** Topographically corrected CPR image of Mini-RF swath LSZ\_03737\_2CD\_OKU\_90S137\_V1 giving location of three annular regions of interest (ROIs).



**Figures 3b-d.** Modified quantile box plots of CPR values vs. local incidence angle for three regions of interest given in Fig 3a: (3b) upper ROI; (3c) middle ROI; (3d) inner/lower ROI.

CPR values in each of these regions of interest (ROI) are plotted relative to local incidence angle as determined from the LOLA gridded topographic data (Fig. 3b-d). Due to the large degree of scatter, the results are presented as modified quantile box plots. The

results are binned into  $1^\circ$  increments, and the center point of each bin is the median value. Error bars represent  $\pm 25\%$  (i.e., the 25<sup>th</sup> and 75<sup>th</sup> percentile values).

From these comparisons, it is apparent that CPR values decrease with depth into the crater, at least for local incidence angles  $< 30^\circ$ . Although there are numerous pixels with CPR values in excess of unity, they have a heterogeneous distribution throughout the crater.

**Implications for Lunar Volatiles:** High CPR values observed within Shackleton are patchy and non-uniform. While these are consistent with a heterogeneous mixture of ice and silicate regolith, other effects such as roughness cannot be ruled out. It has long been recognized, for example, that steep surfaces do not accumulate regolith in the same manner as flat areas, and thus relatively fresh exposures of crater wall rock may yield higher than average decimeter-scale surface roughness. At this point, the new radar data simply confirm that large expanses of slab-like ice are not present within Shackleton.

Despite this as-yet-unresolved ambiguity, Shackleton crater remains a viable candidate site of polar volatile accumulation when viewed in conjunction with other data. The interior of Shackleton is in permanent shadow, and the thermal environment measured by the DIVINER instrument indicates that temperatures are low enough for solid water ice to be stable [12]. The LCROSS impact detected a faint signature of water vapor in the nearby Cabeus region [13], results from Lunar Prospector and LRO's LEND suggest polar concentrations of excess hydrogen [14, 15], and Moon Mineralogy Mapper ( $M^3$ ) data indicate poleward concentrations of hydroxyl and/or water [16]. Quantifying the specific sites of volatile accumulation remains elusive, but the Mini-RF team continues to further characterize these and other locations.

**References:** [1] Bussey D.B.J. et al. (2010) *Icarus*, 208, 558-564. [2] Watson K. et al. (1961) *JGR*, 66, 1598-1600. [3] Arnold J.R. (1979) *JGR*, 84, 5659-5668. [4] Crider D.H. & Vondrak R.R. (2003) *JGR*, 108, 5079. [5] Spudis P.D. et al. (2008) *GRL*, 35, 14201. [6] Nozette S. et al. (1996) *Science*, 274, 1495-1498. [7] Stacy N.J.S. et al. (1997) *Science*, 278, 145. [8] Campbell D.B. et al. (2006) *Nature*, 443, 835-837. [9] Raney R.K. (2007) *IEEE TGRS*, 45, 3397-3404. [10] Nozette S. et al. (2010) *Space Sci. Rev.*, 150, 285-302. [11] Smith D.E. et al. (2010) *GRL*, 37, 18204. [12] Paige D.A. et al. (2010) *Science*, 330, 479-482. [13] Colaprete A. et al. (2010) *Science*, 330, 463-468. [14] Lawrence D.J. et al. (2006) *JGR*, 111, 08001. [15] Mitrofanov I.G. et al. (2010) *Science*, 330, 483-486. [16] Pieters C.M. et al. (2009) *Science*, 326, 568-572.